Nanoscale

Accepted Manuscript

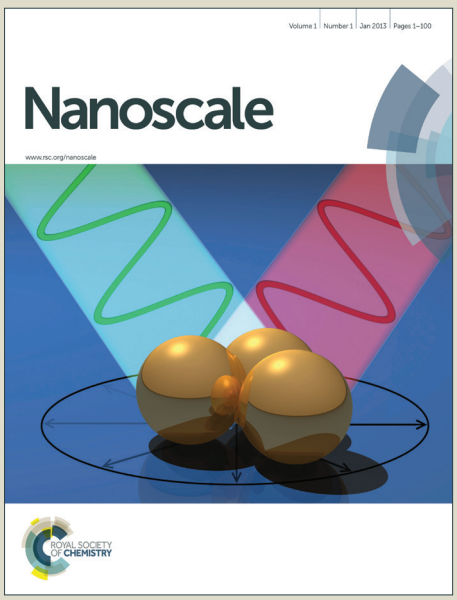

ROYAL SOCIETY OF CHEMISTRY

www.rsc.org/nanoscale

Nanoscale

RSCPublishing

COMMUNICATION

Efficient Synthesis of $Au_{99}(SR)_{42}$ Nanoclusters

Cite this: DOI: 10.1039/x0xx00000x

Chao Liu, Jizhi Lin, Yangwei Shi and Gao Li*

Received 00th January 2012,
Accepted 00th January 2012

DOI: 10.1039/x0xx00000x

www.rsc.org/

We report a new synthetic protocol of the $Au_{99}(SPh)_{42}$ nanoclusters with good efficiency (~15% yield based on the $HAuCl_4$), via a combination of the ligand-exchange and "size-focusing" process. The purity of the as-prepared gold nanoclusters is characterized by matrix-assisted laser desorption ionization mass spectrometry and size exclusion chromatography.

Atomically precise gold nanoclusters have emerged as one of the most important types of nanomaterials that are being extensively explored in nanoscience and nanotechnology research.[1-4] The gold nanoclusters, formulated as $Au_n(SR)_m$ (SR represent the thiolate ligand), are ideally composed of an exact number of gold atoms (*n*, ranging from ten to a few hundred of atoms) and protecting thiolate ligands (*m*); their size typically ranges from subnanometer to ~2 nm (core diameter). Due to quantum size effects of this extremely small size regime, the gold nanoclusters possess unique physical and chemical properties, making this type of nanomaterial very promising in optical properties and photovoltaics, as well as applications in fields such as catalysis and biology.[5-13]

There are main two protocols for the wet chemical synthesis of the atomically precise gold nanoclusters: "size-focusing" and ligand-exchange. In respect of the "size-focusing" process, a proper distribution of polydispersed gold nanoclusters, the key point, is made by kinetically controlling the reduction of gold precursor (typically Au(I)-SR polymer) with $NaBH_4$ reducing agent. The as-prepared polydispersed gold nanoclusters are subjected to "size-focusing" under relatively harsh conditions (e.g., at 80 ^oC and in the presence of excess thiol). During the "size-focusing" process, the unstable gold nanoclusters decompose/convert to the thermostable gold nanoclusters, and eventually give rise to only the most thermostable gold nanoclusters.[14-17] On the other hand, in the ligand-exchange method, the new gold nanoclusters was synthesized via replacing the protecting thiolate ligands on the parent gold nanoclusters with other ligands; of note, some of the size of the new formed nanoclusters (i.e., the number *n*) would be changed.[18-20] Although major advances in the wet chemical synthesis (e.g., size-focusing processes and ligand-exchange) of the gold nanoclusters at the atomic level have been achieved (such as $Au_{25}(SR)_{18}$, $Au_{36}(SR)_{24}$, $Au_{38}(SR)_{24}$, $Au_{144}(SR)_{60}$, etc),[21-26] only a few can be obtained in bulk quantity with high purity and high yield by facile synthetic methods.[15-17] For example, Shichibu *et al*. reported the synthesis of $Au_{25}(SG)_{18}$ nanoclusters from the parent phosphine-capped Au_{11} clusters (i.e., $Au_{11}(PPh_3)_7Cl_3$) by ligand-exchange at 55 ^oC.[15] Meanwhile, Murry and coworkers obtianed the $Au_{\sim 75}(SR)_{\sim 40}$ (where, SR = SC_6H_{13} and SC_2H_4Ph) nanoclusters by ligand-exchange of $Au_{55}(PPh_3)_{12}Cl_6$.[17] And in very recently, Zeng *et al.* also reported the synthesis of $Au_{36}(SPh^tBu)_{24}$ nanoclusters by ligand-exchange of $Au_{38}(SC_2H_4Ph)_{24}$ in the presence of excess $HSPh^tBu$ ligand under a thermal condition.[22] Qian *et al*. synthesized $Au_{38}(SC_{12}H_{25})_{24}$ nanoclusters via ligand-exchange of the polydispersed $Au_n(SG)_m$ (SG = glutathionate, 38< n <102) with dodecanethiol ($HSC_{12}H_{25}$) at 80 ^oC overnight.[23] In all, to obtain bulk quantity and high yield, the polydispersed gold nanoclusters with narrow and suitable mass distribution are the key step in the synthesis of the atomically precise gold nanoclusters.

In our previous work, we reported the synthesis and catalytic application of the $Au_{99}(SPh)_{42}$ nanoclusters.[27] The $Au_{99}(SPh)_{42}$ nanoclusters showed very high catalytic performance in the chemoselectivity hydrogenation of nitrobenzaldehyde into nitrobenyl alcohol, however the yield of the Au_{99} nanoclusters is relative low (~1% based on the $HAuCl_4$ salt). Of note, the synthesis of $Au_{99}(SPh)_{42}$ nanoclusters was via only "size-focusing" of the polydisperse $Au_n(SPh)_m$ in the presence of excess thiophenol (H-SPh) without ligand-exchange.[27] In this work, we report a bulk solution synthetic protocol that permits facile, large scale synthesis of monodisperse $Au_{99}(SPh)_{42}$ nanoclusters with high purity. This new protocol explores a ligand-exchange process in which *n*-hexanethiolate-protected polydispersed $Au_n(SC_6H_{13})_m$ nanoclusters (the mass distribution of the clusters mainly focus on *m/z* ~25k) are utilized as the starting material. Then thiophenol causes the gold core etching and secondary size-focusing of gold

nanoclusters, ultimately resulting in monodisperse $Au_{99}(SPh)_{42}$ nanoclusters in high purity with a good yield (~15% based on $HAuCl_4 \cdot 3H_2O$).

In a typical experiment, the synthesis of $Au_{99}(SPh)_{42}$ nanoclusters involves two major steps, i) synthesis of the polydispersed $Au_n(SC_6H_{13})_m$ nanoclusters and ii) thiol ligand-exchange induces growth of the $Au_{99}(SPh)_{42}$ nanoclusters from the $Au_n(SC_6H_{13})_m$ mixture. Briefly, the polydispersed $Au_n(SC_6H_{13})_m$ nanoclusters are obtained via the $NaBH_4$ reduction of the THF solution of the Au:(SC_6H_{13}) polymer at the thiol/Au ratio of 3.0. The $Au_n(SC_6H_{13})_m$ nanoclusters is then subject to ligand-exchange using neat thiophenol (see the ESI† for details). In this work, we use excess thiophenol to effect core etching of $Au_n(SC_6H_{13})_m$ nanoclusters during the ligand exchange process, and finally attain highly pure $Au_{99}(SPh)_{42}$ nanoclusters. The other sized clusters in the original materials should be decomposed or change to $Au_{99}(SPh)_{42}$ nanoclusters; for example, the $Au_{25}(SR)_{18}$ nanoclusters was decomposed under thermal etching (e.g., 80 °C) in an air atmosphere, although it was relatively stable under N_2 atmosphere.

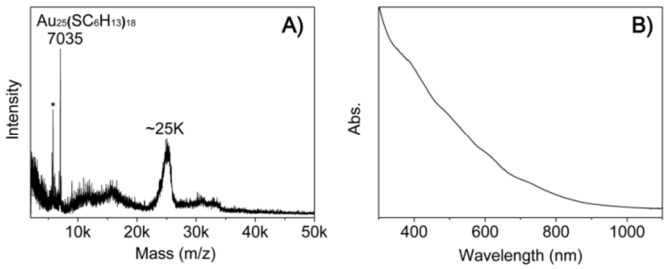

Figure 1. (A) The MALDI mass spectrum of the starting materials (i.e., the polydispersed $Au_n(SC_6H_{13})_m$ nanoclusters). $Au_{25}(SC_6H_{13})_{18}$ nanoclusters (m/z: 7,035) was found in the mass spectrum; of note, the peak marked with an asterisk (*) is a fragment (i.e., $Au_{21}(SC_6H_{13})_{14}$ species) of $Au_{25}(SC_6H_{13})_{18}$. (B) UV-vis spectrum of the as-prepared $Au_{99}(SPh)_{42}$ nanoclustsers.

A decay curve is observed in the UV-vis spectrum, indicating that the starting materials (i.e., $Au_n(SC_6H_{13})_m$ nanocluster mixture) are polydispersed, in consistent with the matrix-assisted laser desorption ionization mass spectrometric (MALDI-MS) analysis (Figure 1A). A single peak centered at *m/z* 7,035 is belonged to $Au_{25}(SC_6H_{13})_{18}$ nanoclusters (theoretical mass: 7,034.4); of note, the weak single peak at *m/z* 5,777 is a fragment ($Au_{21}(SC_6H_{13})_{14}$ species, losing one $Au_4(SC_6H_{13})_4$ unit) of the $Au_{25}(SC_6H_{13})_{18}$ nanoclusters due to the MALDI method, in consistent with the previous reported literatures.[25] Another strong broaden peak centered at *m/z* ~25k (k = 1,000) is found in the mass spectrum, assigned to $Au_{\sim 100}$:SC_6H_{13} nanoclusters. Additionally, some other weak broaden peaks (*m/z* from 10k to 20k, and 30k to 35k) also existed in the $Au_n(SC_6H_{13})_m$ nanocluster mixture (Figure 1A). After 8h etching in the presence of the excess thiophenol at 80 °C, a new gold nanoclusters with a characteristic feature is obtained; same multi-bands are shown at 730, 600, 490, and 400 nm in the range from 300 to 1100 nm (Figure 1B), in consistent with the reported $Au_{99}(SPh)_{42}$ nanoclusters.[27,29]

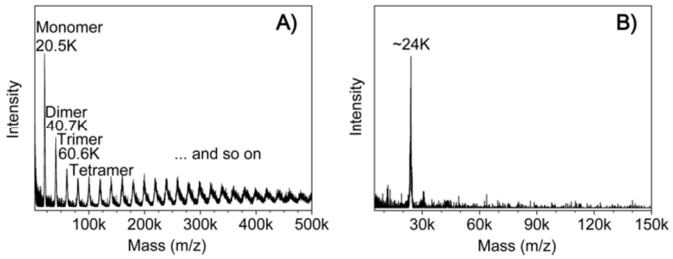

Figure 2. (A) LDI and (B) MALDI mass spectra of the as-prepared $Au_{99}(SPh)_{42}$ nanoclusters.

To identify the purity of the as-prepared Au nanoclusters, we first check the sample by laser desorption ionization (LDI) and matrix-assisted laser desorption ionization (MALDI) mass spectrometric analysis. Of note, the sample, special large molecules (e.g., the molecular weight reaches to 20K), tends to be fragile and fragment under the high laser intensity in both of the LDI and MALDI analysis. As shown in Figure 2A, the LDI mass spectrum shows a series of peaks with equal spacing of ~20k. The first peak is at *m/z* 20.5k (singly charged), which is mainly from the cluster core (in the ionized form, $\sim Au_{99}S_{42}$ species: theoretical *m/z* 20,845). The peaks at *m/z* 40.7, 60.6, 80.5, and 100.4k (and so on) are corresponding to the dimer, trimer, tetramer, and pentamer ions (and so on, all singly charged) of the 20.5k primary ion, respectively; note that these oligomers are only formed in *gas phase* during the LDI process, rather than being present in the original product. Further, we performed the MALDI-MS analysis using *trans*-2-[3-(4-tertbutylphenyl)-2-methyl-2-propenylidene] malononitrile (DCTB) as a matrix; note that the MALDI method is much softer than LDI. Unlike in the LDI, only one dominant peak at *m/z* ~24.0k is found (Figure 2B) and assigned to the $Au_{99}(SPh)_{42}$ or $Au_{99}(SPh)_{41}$ species (theoretical *m/z* 24,084 or 23,975); note that one –SPh loss also was observed in the case of the $Au_{36}(SPh)_{24}$ nanoclusters.[27] The 24.0k value is much higher in mass than the LDI-determined *m/z* 20.5k, implying that the loss of the tail of thiolate ligand (i.e., -Ph) occurrs in the LDI process, which is due primarily to the breaking of S–C bonds and loss of -Ph fragments (even some Au–S bonds also are ruptured). There is no gas-phase dimer, trimer, tetramer, and pentamer species in the MALDI

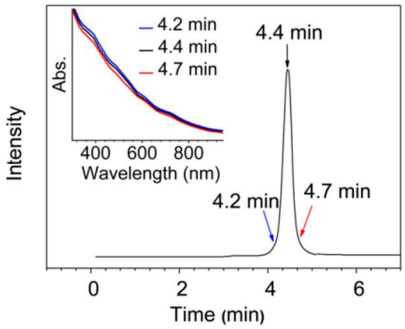

Figure 3. Size-exclusion chromatogram of the as-obtained $Au_{99}(SPh)_{42}$ nanoclusters (monitored at λ = 500 nm using CH_2Cl_2 (0.5 mL/min) as

the eluent). Inset: online-recorded UV–vis spectra corresponding to the different retention times.

process (Figure 2B), consistent with our precious work.[27] Thus, DCTB matrix can largely suppress the loss of -Ph tail from the ionized nanocluster as well as the gas-phase oligomerization. Nevertheless, both the above wide-range LDI and MALDI mass spectra clearly demonstrate that the as-synthesized $Au_{99}(SPh)_{42}$ nanoclusters are highly uniform.

Size exclusion chromatography (SEC) has been successfully applied in the confirmation of the purity of gold nanoclusters.[30-32] A diode array detector (DAD) *in situ* monitors (at λ = 500 nm) the UV-Vis spectra of eluted Au nanonclusters. Figure 3 shows only one single symmetric peak; the inset shows the optical spectra (300–950nm) corresponding to the eluted components at 4.2 min (left side of the peak), 4.4 min (the peak position), and 4.7 min (right side of the peak), respectively. The three optical spectra are indeed superimposable, further indicating high purity of the as-prepared $Au_{99}(SPh)_{42}$ nanoclusters. And further, thermal gravimetric analysis (TGA) is also tested (Figure 4), which shows a weight loss of 18.9 wt% (corresponding to the losing of the surface thiolate ligands), consistent with the expected value (19.0 wt%) according to the $Au_{99}(SPh)_{42}$ formula and the previous work.[27] In all, the above characterizations also strongly indicate that the as-obtained $Au_{99}(SPh)_{42}$ nanocluster samples are highly uniform.

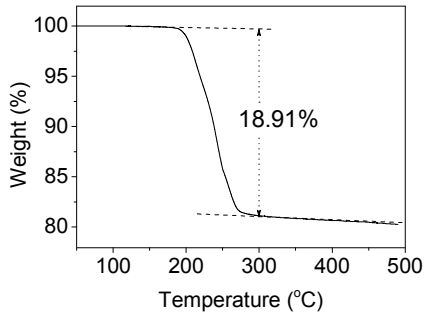

Figure 4. TGA curve of the as-prepared Au nanoclusters in N_2 atmosphere.

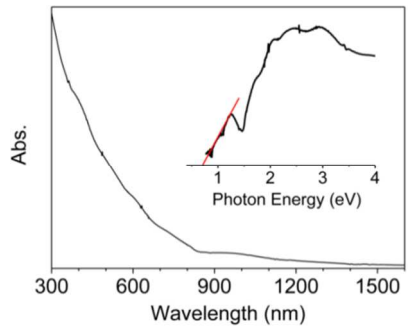

Figure 5. UV-vis-NIR spectrum (range from 300 to 1600 nm) of $Au_{99}(SPh)_{42}$ nanocluster. (Inset) The spectrum on the energy scale (eV); the HOMO-LUMO gap of the $Au_{99}(SPh)_{42}$ nanoclusters is ~0.71 eV (see red intercept).

Further, we investigate the UV-vis-NIR spectrum (range from 300 to 1600 nm) of the pure $Au_{99}(SPh)_{42}$ nanoclusters, and found that a new broad peak appeared at ~920 nm (1.35 eV), as shown in Figure 5. Therefore, five optical peaks, 920 (1.35), 730 (1.70), 600 (2.07), 490 (2.53), and 400 nm (3.10 eV), are observed in the $Au_{99}(SPh)_{42}$ nanoclusters. By extrapolating the optical absorbance to zero, the HOMO-LUMO gap of $Au_{99}(SPh)_{42}$ nanoclusters is determined to be ~0.71 eV (Figure 5, inset).

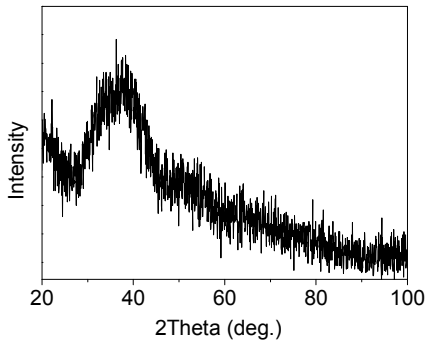

Figure 6. Powder XRD of the $Au_{99}(SR)_{42}$ nanoclusters.

We perform powder X-ray diffraction (XRD) analysis to investigate the atomic structure of the $Au_{99}(SPh)_{42}$ nanoclusters. As shown in the Figure 6, a peak centered at 2θ ~39^o is observed, which is similar with that of Au_{102}. Therefore, it is predicted that the Au_{99} cluster exhibits a similar Marks decahedral core and should be composed of $Au_{78}(Au(SR)_2)_{21}$ or $Au_{77}(Au(SR)_2)_{18}(Au_2(SR)_3)_2$ as only the [–SR–Au–SR–] and [–SR–Au–SR–Au–SR–] type staples are found in the large Au nanoclusters (e.g., $Au_{102}(SR)_{44}$, $Au_{79}(Au(SR)_2)_{19}(Au_2(SR)_3)_2$).[33-35] Noted that theoretical calculations and growth of single crystal of the $Au_{99}(SR)_{42}$ nanoclusters can facilitate the understanding of its structure.

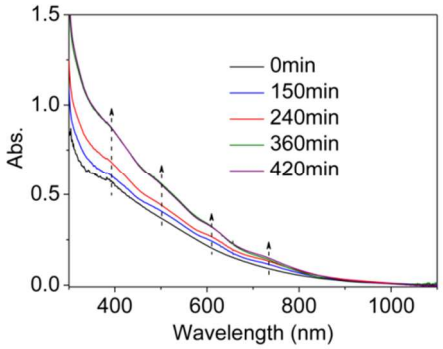

Figure 7. Time-dependent UV–vis spectral evolution of thiophenol (PhSH) reaction with $Au_n(SC_6H_{13})_m$ nanoclusters.

Finally, we investigate the conversion process from the starting material-$Au_n(SC_6H_{13})_m$ to the pure $Au_{99}(SPh)_{42}$ nanoclusters by monitoring with UV-vis spectroscopy in the toluene solution at 80 ^{o}C for 420 mins (other conditions: 0.1 mg $Au_n(SC_6H_{13})_m$ and 5 μL PhSH in a closed cuvette). As seen in the Figure 7, the multi-bands at 730, 600, 490, and 400 nm are appeared after ~150 mins, and the relative intensity of these bands gradually increase, indicating that the other sized gold nanoclusters disappeared (e.g.,

decomposed or change to the $Au_{99}(SPh)_{42}$ nanoclusters) and the sample finally gives rise to the thermstable $Au_{99}(SPh)_{42}$. The UV-vis spectra of the sample at 360 and 420 mins are superimposable, clearly suggesting that only the $Au_{99}(SPh)_{42}$ nanoclusters is survived under the harsh "size-focusing" conditions.

In summary, we successfully synthesize the atomically precise $Au_{99}(SPh)_{42}$ nanoclusters with good efficiency (~15% yield based on the $HAuCl_4$). The synthetic protocol is mainly via two steps: i) the ligand-exchange and ii) the "size-focusing" process from the starting materials (polydispersed $Au:SC_6H_{13}$ nanoclusters with a mass at *m/z* ~25k) in the presence of excess thiophenol at 80 ^oC overnight. The whole process further is monitored by UV-vis spectroscopy. The as-prepared $Au_{99}(SPh)_{42}$ nanocluters is fully checked by laser desorption ionization and matrix-assisted laser desorption ionization mass spectroscopy, thermal gravimetric analysis, and the size exclusion chromatography. Multi-bands, ~920 (1.35), 730 (1.70), 600 (2.07), and 490 nm (2.53 eV), are observed in the optical absorption spectrum of $Au_{99}(SPh)_{42}$ in the range from 300 to 1600 nm. The HOMO-LUMO gap of the $Au_{99}(SPh)_{42}$ nanoclusters is approximately 0.71 eV.

Acknowledgements

This work was partially supported by the starting funds of the Dalian Institute of Chemical Physics and the "Thousand Youth Talents Plan".

Notes and references

State Key Laboratory of Catalysis & Gold Catalysis Researcher Centre, Dalian Institute of Chemical Physics, Chinese Academy of Sciences, Dalian 116023, China.
*E-mail: gaoli@dicp.ac.cn

Electronic Supplementary Information (ESI) available: [Experimental Section: the synthetic procedure of the $Au_{99}(SPh)_{42}$ nanoclusters and characterization of the Au cluster]. See DOI: 10.1039/c000000x/

1 H. Qian, M. Zhu, Z. Wu and R. Jin, *Acc. Chem. Res.*, 2012, **45**, 1470–1479.
2 R. Jin, *Nanoscale*, 2015, **7**, 1549–1565.
3 R. L. Whetten, M. N. Shafigullin, J. T. Khoury, T. G. Schaaff, I. Vezmar, M. M. Alvarez and A. Wilkinson, *Acc. Chem. Res*., 1999, **32**, 397–406.
4 G. Schmid, *Chem. Soc. Rev*., 2008, **37**, 1909–1930.
5 S. Yau, O. Varnavski and T. Goodson, *Acc. Chem. Res*., 2013, **46**, 1506–1516.
6 B. Unnikrishnan, S. Wei, W. Chiu, J. Cang, P. Hsu and C. Huang, *Analyst*, 2014, **139**, 2221–2228.
7 M. Wang, Z. Wu, J. Yang, G. Wang, H. Wang and W. Cai, *Nanoscale*, 2012, **4**, 4087–4090.
8 Z. Wu, M. Wang, J. Yang, X. Zheng, W. Cai, G. Meng, H. Qian, H. Wang and R. Jin, *Small*, 2012, **13**, 2028–2035.
9 G. Li, H. Qian and R. Jin, *Nanoscale*, 2012, 4, 6714–6717.
10 N. Sakai and T. Tatsuma, *Adv. Mater*., 2010, **22**, 3185–3188
11 A. Mathew, G. Natarajan, L. Lehtovaara, H. Häkkinen, R. M. Kumar, V. Subramanian, A. Jaleel and T. Pradeep, *ACS Nano*, 2014, **8**, 139–152.
12 G. Li and R. Jin, *Acc. Chem. Res*., 2013, **46**, 1749–1758.
13 G. Li, D. Jiang, C. Liu, C. Yu and R. Jin, *J. Catal*., 2013, **306**, 177–183.
14 R. Jin, H. Qian, Z. Wu, Y. Zhu, M. Zhu, A. Mohanty and N. Garg, *J. Phys. Chem. Lett.*, 2010, **1**, 2903–2910.
15 Y. Shichibu, Y. Negishi, T. Tsukuda and T. Teranishi, *J. Am. Chem. Soc*., 2005, **127**, 13464–13465.
16 P. Maity, S. Xie, M. Yamauchi and T. Tsukuda, *Nanoscale*, 2012, **4**, 4027–4037.
17 R. Balasubramanian, R. Guo, A. J. Mills and R. W. Murray, *J. Am. Chem. Soc*., 2005, **127**, 8126–8132.
18 S. Si, C. Gautier, J. Boudon, R. Taras, S. Gladiali and T. Bürgi, *J. Phys. Chem. C*, 2009, **113**, 12966–12969.
19 T. W. Ni, M. A. Tofanelli, B. D. Phillips and C. J. Ackerson, *Inorg. Chem*., 2014, **53**, 6500–6502.
20 J. B. Tracy, M. C. Crowe, J. F. Parker, O. Hampe, C. A. Fields-Zinna, A. Dass and R. W. Murray, *J. Am. Chem. Soc*., 2007, **129**, 16209–16215.
21 D. Crasto, S. Malola, G. Brosofsky, A. Dass and H. Häkkinen, *J. Am. Chem. Soc*., 2014, **136**, 5000–5005.
22 C. Zeng, C. Liu, Y. Pei and R. Jin, *ACS Nano*, 2013, **7**, 6138–6145.
23 H. Qian, M. Zhu, U. N. Andersen and R. Jin, *J. Phys. Chem. A*, 2009, **113**, 4281–4284.
24 H. Qian and R. Jin, *Nano Lett*., 2009, **9**, 4083–4087.
25 M. Zhu, E. Lanni, N. Garg, M. E. Bier and R. Jin, *J. Am. Chem. Soc*., 2008, **130**, 1138–1139.
26 Q. Zhang, J. Xie, Y. Yu and J. Y. Lee, *Nanoscale*, 2010, **2**, 1962–1975
27 G. Li, C. Zeng and R. Jin, *J. Am. Chem. Soc.*, 2014, **136**, 3673–3679.
28 G. Li and R. Jin, *J. Am. Chem. Soc*., 2014, **136**, 11347–11354.
29 P. R. Nimmala and A. Dass, *J. Am. Chem. Soc.*, 2014, **136**, 17016–17023.
30 A. M. Al-Somali, K. M. Krueger, J. C. Falkner and V. Colvin, *Anal. Chem*., 2004, **76**, 5903–5910.
31 G. Wei and F. Liu, *J. Chromatogr. A*, 1999, **836**, 253–260.
32 H. Qian, Y. Zhu and R. Jin, *J. Am. Chem. Soc*., 2010, **132**, 4583–4585.
33 P. D. Jadzinsky, G. Calero, C. J. Ackerson, D. A. Bushnell and R. D. Kornberg, *Science*, 2007, **318**, 430–433.
34 A. Dass, P. R. Nimmala, V. R. Jupally and N. Kothalawala, *Nanoscale*, 2013, **5**, 12082–12085.
35 Y. Gao, N. Shao and X. C. Zeng, *ACS Nano*, 2008, **2**, 1497–1503.

TOC: